Chapter III

SIMULATION INSIDE BIOFILM

Simple Prediction of Oxygen Penetration Depth in Biofilms for Wastewater Treatment

3.1 INTRODUCTION

In this chapter, oxygen concentration in the biofilms of several thicknesses was measured using an oxygen microelectrode, and was statistically simulated by the finite difference method at several biofilm thicknesses and bulk oxygen concentrations. The kinetic parameters and effective diffusion coefficients of oxygen in the biofilm, and the oxygen penetration depths were determined. As a result, the optimum thickness of the biofilms for oxidizing processes such as simultaneous organic carbon removal and nitrification in a fluidized bed reactor was determined.

3.2 MATERIALS AND METHODS

3.2.1 Simulation

The oxygen distribution in the biofilms was simulated with a Monod equation with regard to oxygen consumption through biological reaction. The parameters were determined in accordance with the method of Lewandowski [25]. The calculation method is as follows: The mass balance equation for oxygen in the biofilms is

$$\frac{dC}{dt} = D_e \frac{d^2C}{dx^2} - \frac{k \cdot X \cdot C}{K_m + C}, \qquad (1)$$

where C is the oxygen concentration, t the time, D_e the effective diffusion coefficient of oxygen in the biofilms, x the distance from the biofilm surface, k the reaction rate constant, K_m the Monod saturated constant, and X the dry density of the biofilms. When the steady-state concentration profile of the inside of a biofilm is achieved, the consumption rate is equal to diffusion rate. Then, taking the inverse of each part in Equation (1) yields the function between the inverse of the second derivative and the inverse of oxygen concentration as

$$\left(\frac{d^2C}{dx^2}\right)^{-1} = \frac{D_e \cdot K_m}{k \cdot X} \cdot \frac{1}{C} + \frac{D_e}{k \cdot X}. \qquad (2)$$

The slope ($D_e \cdot K_m / k \cdot X$) divided by the intercept ($D_e / k \cdot X$) yields K_m. The second derivative is calculated using the exponential equation (Equation (3)) that fits to the experimental profile of oxygen distribution in the biofilms. The exponential equation was best fitted for the experimental data.

$$C = a_1 + a_2 \cdot \exp(-x / a_3) \qquad (3)$$

According to Frank-Kameneski [26], the mass balance equation at the steady state can be transformed to

$$\left(\frac{dC}{dx}\right)_f = \sqrt{2\frac{k \cdot X}{D_e}\left(C - K_m \cdot \ln\frac{K_m - C}{K_m}\right)}, \qquad (4)$$

where subscript f indicates film and $(dC/dx)_f$ is the gradient of oxygen concentration in the biofilm. Using the sets of parameters $k \cdot X/D_e$ and K_m which were computed using Equation (2), the first derivative of oxygen concentration in the biofilm $(dC/dx)_f$ can be obtained.

Substrate molecules, before reaching the biofilm surface, must travel across the diffusion boundary layer. In idealized, perfectly stagnant water, the process would be entirely dependent on molecular diffusion. Consequently, the profile of oxygen concentration would be linear without convection. Therefore, the oxygen profile above the biofilm surface can be adequately described by the empirical exponential function

$$\frac{C - C_s}{C_b - C_s} = 1 - \exp\{-A \cdot (x - x_s)\}, \qquad (5)$$

where subscript s represents the interface between the biofilm and the bulk, subscript b represents the bulk and A is the experimental constant. The first derivative in the bulk $(dC/dx)_w$ is

$$\left(\frac{dC}{dx}\right)_w = A \cdot (C_b - C_s), \qquad (6)$$

where subscript w represents water and $(dC/dx)_w$ is the gradient of oxygen concentration in the bulk. By fitting Equation (5) to the experimental data obtained using the microelectrode, the slope of A is calculated and the first derivative in the bulk $(dC/dx)_w$ can be obtained.

Moreover, oxygen flux through the biofilm-bulk interface (J_f) and diffusion layer (J_w) are respectively defined as

$$J_f = D_f \cdot \left(\frac{dC}{dx}\right)_f, \qquad (7)$$

$$J_w = D_w \cdot \left(\frac{dC}{dx}\right)_w. \qquad (8)$$

Since oxygen flux at the biofilm-bulk interface is continuously preserved ($J_f = J_w$), the

internal diffusion coefficient in the biofilm is given as

$$D_e = D_f = D_w \cdot \frac{\left(\frac{dC}{dx}\right)_w}{\left(\frac{dC}{dx}\right)_f}. \qquad (9)$$

Using the diffusion coefficient of water at 21ºC of 2.0×10^{-9} m^2/s [27], $(dC/dx)_f$ from Equation (4) and $(dC/dx)_w$ from Equation (6), the internal diffusion coefficient of the biofilm, D_e, can be computed. Moreover, k was computed from the calculated values of $k \cdot X/D_e$ and D_e, and the experimental values of X. The average of all the values was represented.

The oxygen distribution is simulated using the calculated kinetics parameters, the dry density of the biofilm and diffusion coefficient of oxygen in the biofilm. The simulation was conducted using Equation (1) by the finite difference method ($dx = 10^{-5}$, $dt = 10^{-7}$, saturation $= 10^{-8}$, and max iterations $= 10^7$). The oxygen distribution inside the biofilm was simulated under the boundary conditions at the biofilm surface and at an infinite point from the biofilm surface. Oxygen penetration depth was determined from the simulation curve of the oxygen distribution in the biofilm.

3.3 RESULTS AND DISCUSSION

3.3.1 Density and porosity

Figure 3.1 shows the plots of dry density against biofilm thickness. Biofilm density decreased with increasing biofilm thickness. The dry density of the biofilm in the fluidized bed reactor was found to be 2-10 times higher than that ($X = 8700$ g/m^3) in the rotating disk reactor [28]. The empirical equation that shows the relation between dry density (X) and biofilm thickness (d) is

$$X = 2.5\times10^4+1.5\times10^5\cdot\exp(-d/175). \qquad (10)$$

Figure 3.2 shows the internal cross-sectional photographs of the biofilms of 120 and 1200 μm thicknesses, obtained using a light microscope. The thin biofilm had a dense homogenous structure. In contrast, the thick biofilm had a heterogeneous structure and large pores. Therefore, the thinner biofilm was expected to exhibit a lower substrate penetration depth because of the high-density structure which results in a small diffusion coefficient and high reaction rate.

3.3.2 Oxygen penetration depth

Using an oxygen microelectrode, the oxygen distribution in the biofilms was measured while maintaining the bulk oxygen concentration at about 3 g/m^3. Examples of the experimental profile and the curves fitted for the exponential equation in the case of biofilms with 425 and 980 μm thicknesses are shown in Figure 3.6. As a result, we found that oxygen was gradually eliminated by bacteria in the biofilm and the liquid film formed in the bulk near the biofilm surface by the reaction. Oxygen penetration depth was determined from the obtainable oxygen distribution in the biofilms. Oxygen penetration ratio was calculated by dividing the oxygen penetration depth by the biofilm thickness. The results of the oxygen penetration depth and ratio are shown in Figure 3.7. Oxygen diffused completely into the bottom of the biofilm of less than 300 μm thickness and oxygen penetration depth increased with increasing biofilm thickness. Oxygen penetration ratio gradually decreased with increasing biofilm thickness. Therefore, there is a large anaerobic zone at the bottom of the thick biofilm, indicating the possibility of microbial denitrification. Pochana et al. [29] considered the denitrification activity in the anaerobic zone in a floc and simulated the distribution of oxygen in the floc. Dalsgaard et al. [30] reported that denitrification activity in the anaerobic zone in a biofilm is computed from the mass balance equation using microelectrode analysis and that the denitrification zone is specified. However, the anaerobic zone is not necessary for oxidation processes such as carbon oxidization and nitrification. The thin biofilm without an anaerobic zone is effective for oxidation processes from the standpoint of obtaining a larger aerobic zone throughout the entire biofilm.

3.3.3 Determination of kinetic parameters and effective diffusion coefficient

Figure 3.3 shows the relationship between $(d^2C/dx^2)_f$ and $1/C$ for evaluating K_m in the case of biofilms of 425 and 980 μm thicknesses. Then, K_m could be calculated from the slope and intercept of the linear fit to the relationship between $(d^2C/dx^2)_f$ and $1/C$. The linear fit for all plots seemed to be impossible, as shown in Figure 4 (b). The linear line could be fitted only for low $1/C$ values, if low oxygen concentrations (below 0.2 g/m^3) are neglected. This concept is reasonable because only high oxygen concentrations affect oxidation rate. Then, the slope, $k \cdot X/D_e \cdot K_m$, and the intercept, $k \cdot X/D_e$, were obtained from the linear fitted curves within the range of the low $1/C$ values. The average K_m calculated from the slope and intercept was 1.5 g/m^3.

The flux at the biofilm surface was calculated using Equation (4). Then, the flux at the diffusion boundary layer was calculated using Equation (5) with the empirical coefficient of A. Figure 3.4 shows an example of the plot for the evaluation of A. Since the flux continuity must be preserved at the biofilm-water interface ($J_f = J_w$), the effective diffusion coefficients were calculated for the distribution of oxygen in each biofilm. Figure 3.5 shows the calculated effective diffusion coefficients plotted against biofilm thickness. The calculated

diffusivity was 40 – 90% which is close to those reported by Stewart et al. [85]. The density-diffusivity correlation was in good agreement with the correlation proposed by Fan et al. [86]. From the result, the empirical equation showing the relationship between D_e and d was obtained.

$$D_e = (3.5^{-19} + 1.5^{-21} \cdot d)^{0.5} \qquad (11)$$

Moreover, k was computed from $k \cdot X/D_e$ (calculated from Figure 3.1), D_e and X (determined from respective empirical equations). The representative k was 7.5×10^{-6} 1/s.

3.3.4 Simulation of oxygen distribution in biofilms

The boundary condition is given by the following equation as the data for oxygen concentration below 0.2 g/m^3 were adopted.

$$\begin{cases} x = x_s; \quad c = c_s \\ x = \infty; \quad c = 0.2 \end{cases} \qquad (12)$$

Figure 3.6 shows the plots of experimental data obtained using the microelectrode and the simulated curves of oxygen distribution in the biofilms of 425 and 980 μm thicknesses. The simulated curves successfully fit the experimental plots. Therefore, the oxygen distribution inside the biofilm can be simulated in the runs where sufficient concentrations of the substrates, that is, organic carbon and ammonia, were supplied, because in such cases, the consumption rates of each substrate and oxygen completely depend on local oxygen concentration. The good fittings indicate that the distribution of the substrate in the biofilm can be sufficiently simulated using a simple model.

Next, oxygen distribution in the biofilms was simulated at several biofilm thicknesses and oxygen concentrations in the bulk. Figure 3.7 shows the experimental plots of oxygen penetration ratio against biofilm thickness and their simulated curves. Therefore, the aerobic zone, which contributes to microbial oxidation, can be predicted at various biofilm thicknesses and oxygen concentrations in the bulk.

3.3.5 Water quality

The water treatment experiment was continuously carried out using the two reactors with the thin (representative biofilm thickness: 120 μm) and thick (representative biofilm thickness: 1200 μm) biofilms. Table 2.2 summarizes the water quality data of the effluent of each reactor in the steady state. The removal efficiency of TOC was high in the reactor with the thin biofilm because oxygen completely diffused into the bottom of the biofilm, and thus all biomass inside the biofilms contributed to the oxidation of organic compounds. In contrast, the removal efficiency of TOC in the reactor with the thick biofilm was lower than that with the thin biofilm, probably because the population of oxidizing bacteria was

relatively small due to the existence of the anaerobic zone inside the biofilm, as determined based on the FISH results (data not shown).

The thin biofilm exhibited a lower nitrification rate than the thick biofilm because there was no space in the bottom zone of the biofilm where the nitrifying bacteria could exist. An adequately thick biofilm is necessary for successful nitrification because of oxygen competition and the distribution of microbial heterotrophs and nitrifiers inside the biofilm. Thus, biofilms of 300 – 400 μm thickness may be appropriate for simultaneous carbon oxidation and nitrification in a fluidized bed reactor. Furthermore, the marked decrease in T-N content indicates that the thick biofilm had denitrification activity in the bottom zone in which oxygen concentration was nearly zero. In a fluidized bed reactor, we suggest that the biofilm thickness should be suitably controlled for objective treatment by aeration which is independent of operation conditions.

3.4 CONCLUSIONS

1. The kinetic parameters of a Monod reaction and the effective diffusion coefficient were calculated based on the oxygen distribution in the biofilms. The effective internal diffusion coefficient of the biofilms changed with biofilm density and biofilm thickness. The effective diffusivity ranged from 40% to 90%.

2. Using the results of biofilm dry density, kinetic parameters and effective diffusion coefficient, the oxygen distribution in the biofilms were successfully simulated using a one-dimensional model with a Monod reaction. It was demonstrated that oxygen penetration ratio, which markedly influences biological oxidation activity, can be determined using this simple simulation.

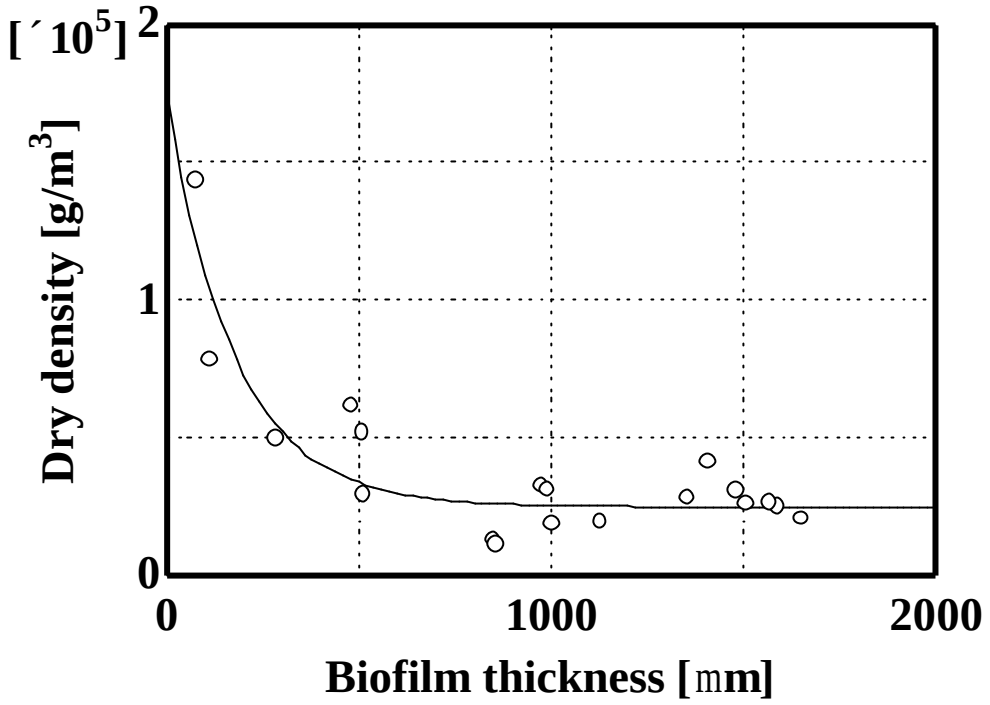

Figure 3.1 Relationship between biofilm thickness and dry density for several biofilm samples (open circles: experimental data; continuous line: smooth curve ($X = 2.5\times10^4 + 1.5\times10^5 \cdot \exp(-d/175)$)

(a) (b)

Figure 3.2 Internal physical structure of (a) thin biofilm (thickness: 120 µm; scale bar denotes 100 µm), and (b) thick biofilm (thickness: 1200 µm; scale bar denotes 500 µm) as observed by light microscopy

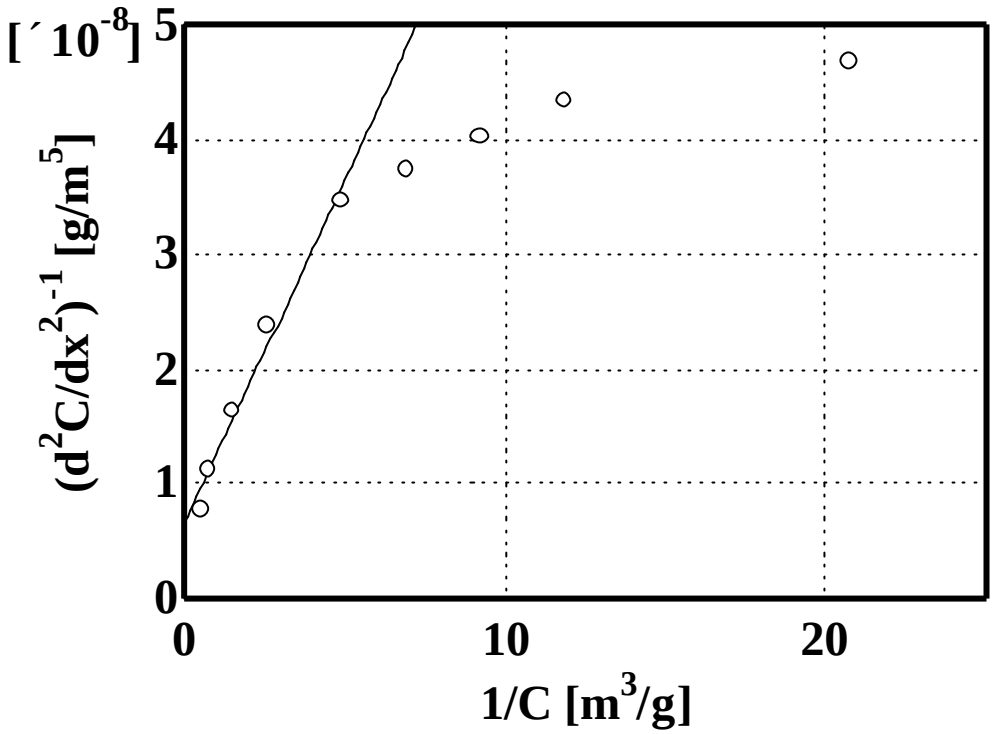

(a)

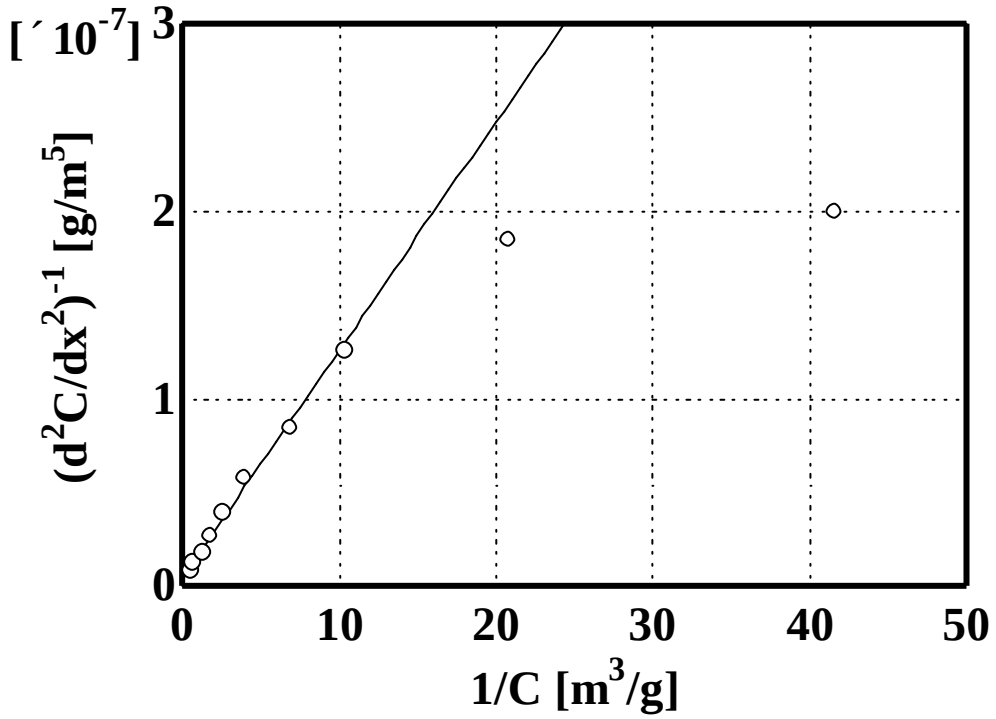

(b)

Figure 3.3 Relationship between $(d^2C/dx^2)_f$ and $1/C$ for evaluating K_m in the case of biofilm of (a) 425 µm and (b) 980 µm thicknesses (open circles: experimental data from microelectrode analysis; continuous line: empirically linear)

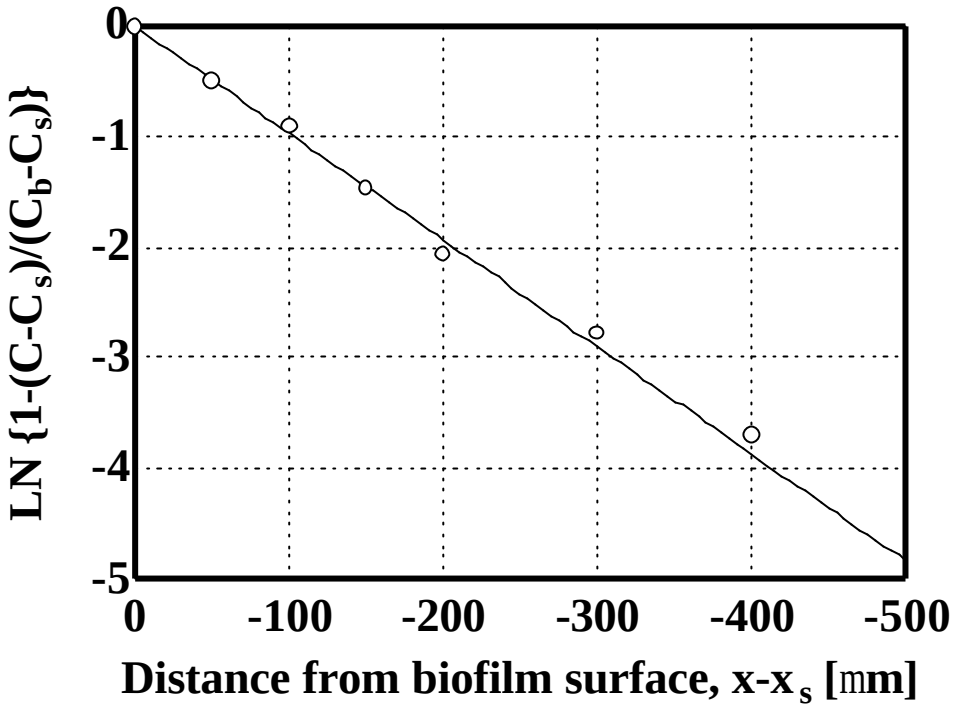

(a)

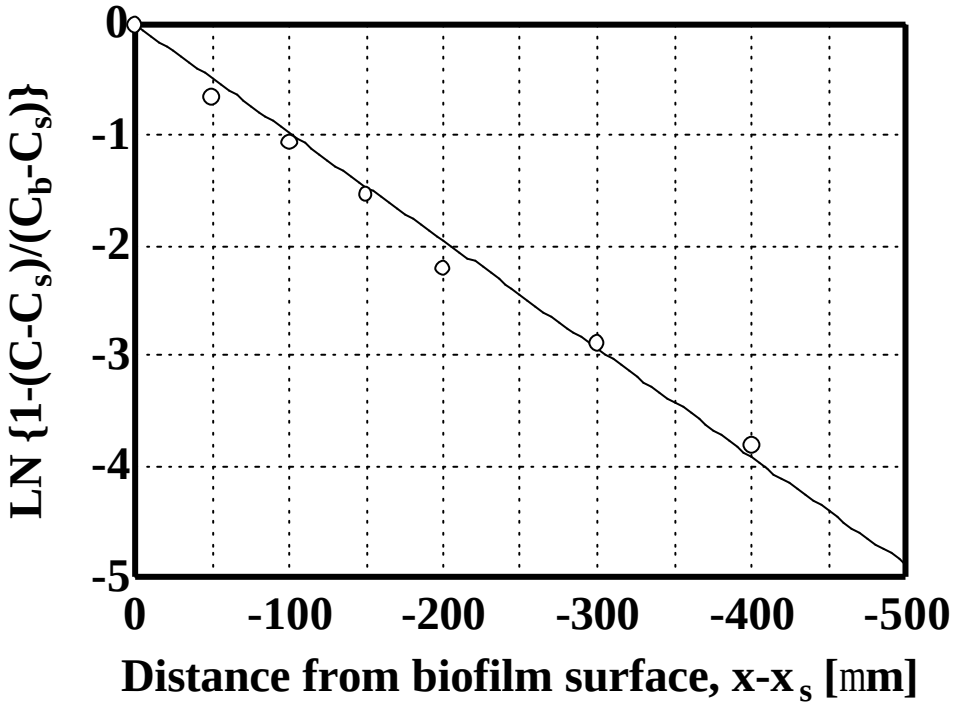

(b)

Figure 3.4 Relationship between LN {1-(C-C_s)/(C_b-C_s)} and distance from biofilm surface, x-x_s, at a diffusion layer in the case of biofilms of (a) 425 µm and (b) 980 µm thicknesses (open circles: experimental data from microelectrode analysis; continuous line: empirically linear)

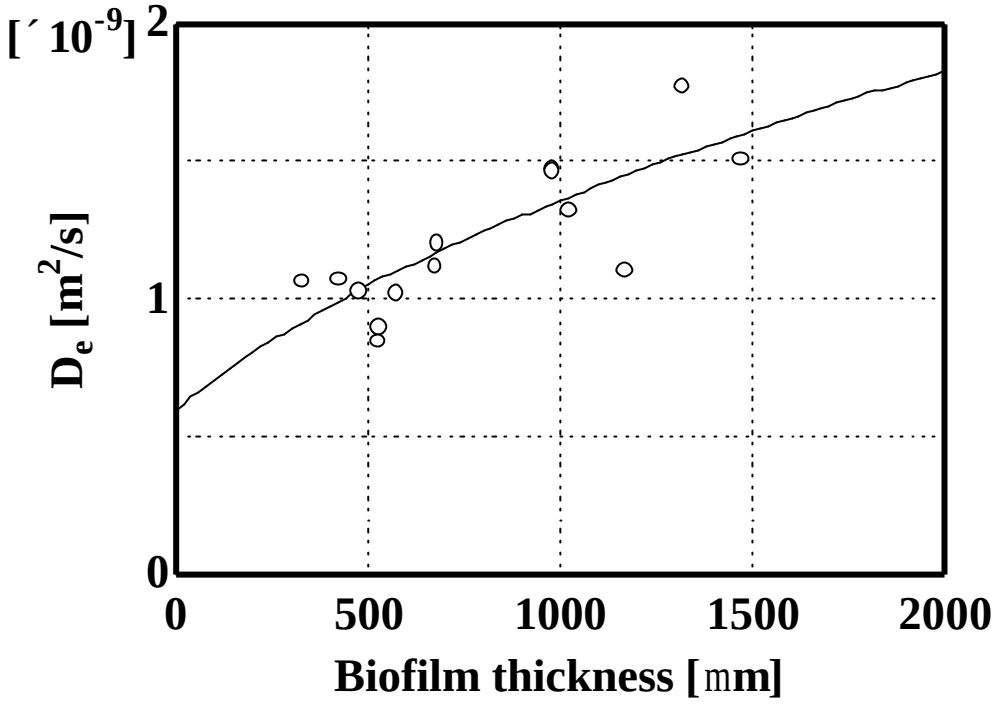

Figure 3.5 Relationship between biofilm thickness and calculated effective diffusion coefficient for several biofilm samples. The empirical equation, $D_e = (3.5^{-19} + 1.5^{-21} \cdot d)^{0.5}$, is shown as a continuous line

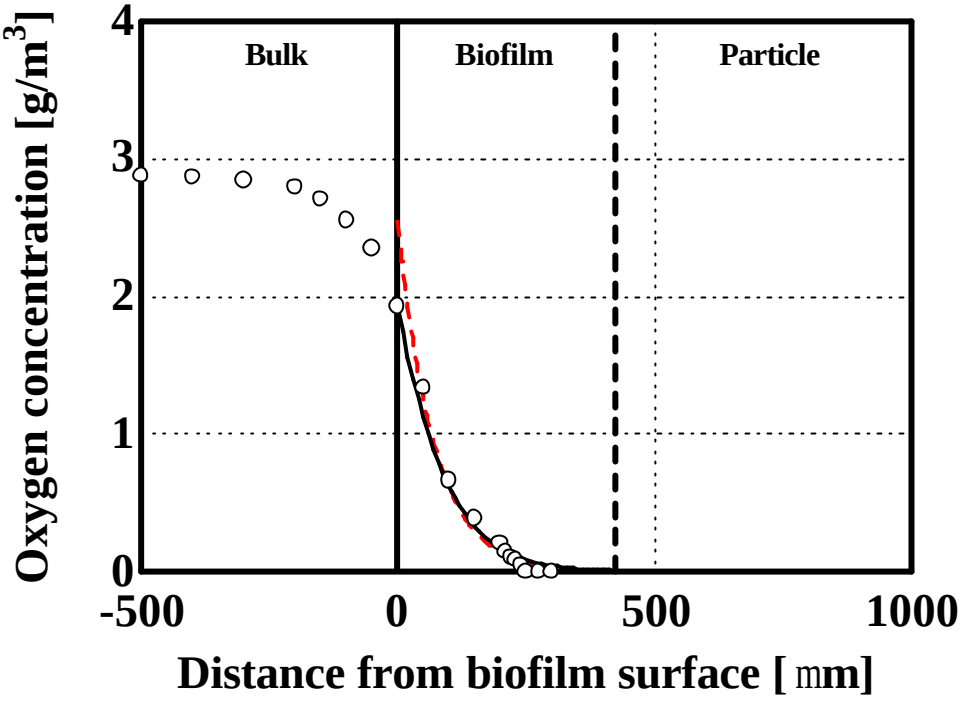

(a)

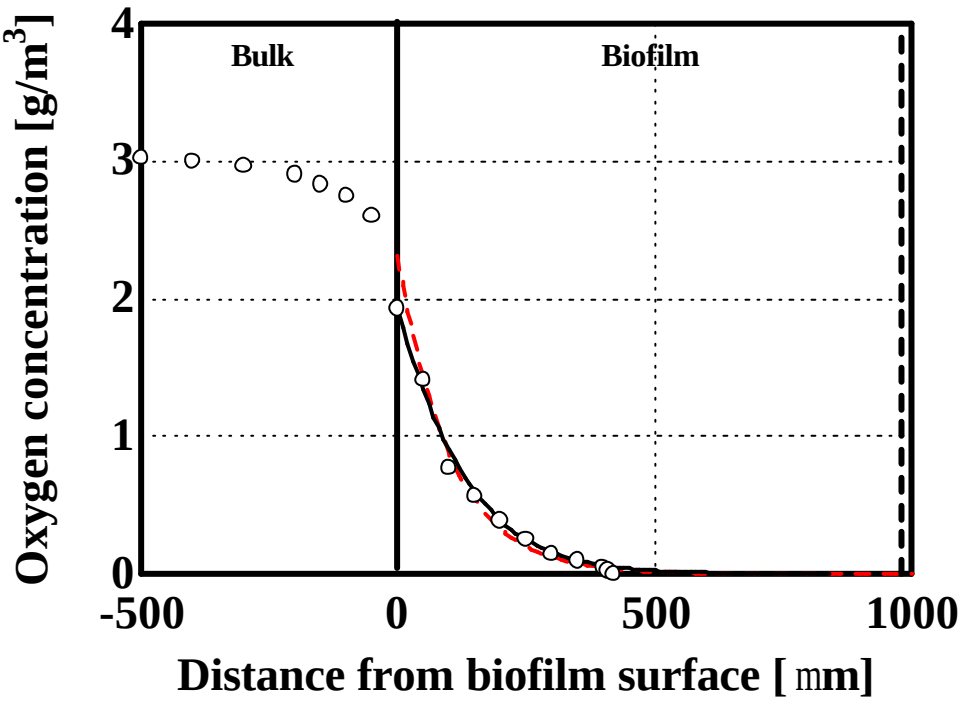

(b)

Figure 3.6 Distribution of oxygen concentration inside biofilms of (a) 425 µm and (b) 980 µm thicknesses (open circles: experimental data from microelectrode analysis; broken line: fitted curve for exponential equation; continuous line: simulated curve)

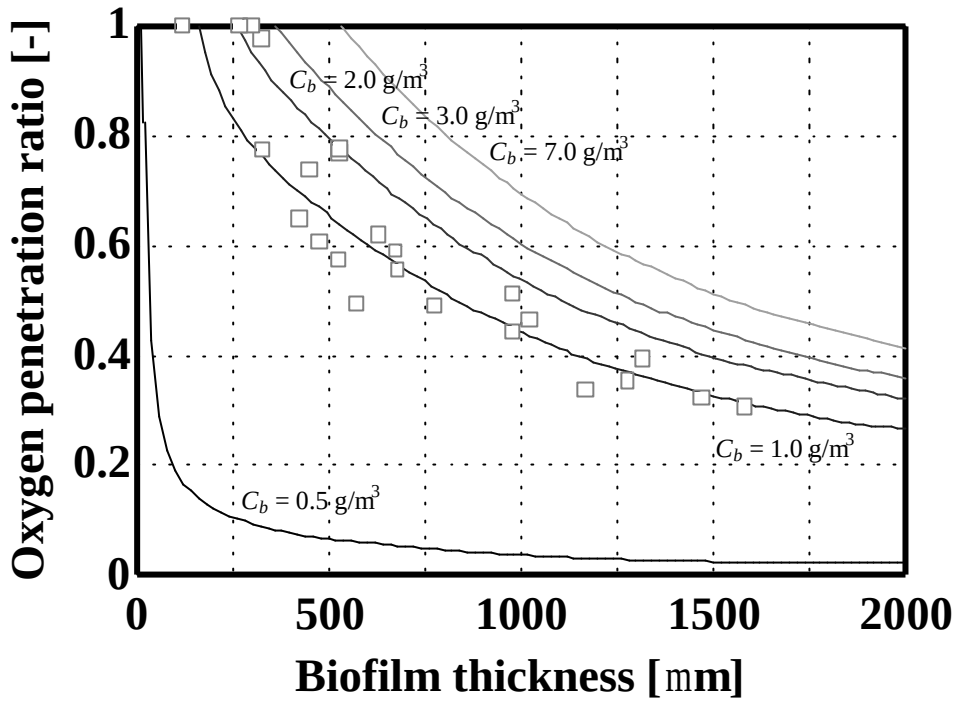

Figure 3.7 Plots of oxygen penetration ratio against biofilm thickness for experimental data obtained at an oxygen concentration of 1.46 – 2.23 g/m^3 at the biofilm surface. Simulated curves are drawn for oxygen concentrations of 0.5 (---), 1.0 (-), 2.0 (-), 3.0 (-) and 7.0 (-) g/m^3 at the biofilm surface

3.5 NOMENCLATURE

a_1 experimental coefficient (-)
a_2 experimental coefficient (-)
a_3 experimental coefficient (-)
A experimental coefficient (-)
C oxygen concentration (g/m^3)
C_0 oxygen concentration at carrier surface (g/m^3)
C_s oxygen concentration at biofilm surface (g/m^3)
C_b oxygen concentration at bulk (g/m^3)
D_e effective diffusion coefficient of oxygen (m^2/s)
D_f diffusion coefficient of oxygen inside biofilm (m^2/s)
D_w diffusion coefficient of oxygen in water (m^2/s)
J_f oxygen Flux inside biofilm ($g/(m^2 \cdot s)$)
J_w oxygen Flux at bulk ($g/(m^2 \cdot s)$)
k reaction constant (1/s)
K_m monod saturated constant (g/m^3)
t time (s)
x distance from carrier surface (m)
x_s distance at biofilm surface (m)
X biofilm density (g/m^3)
d biofilm thickness (m)